Development of HEATHER for Cochlear Implant Stimulation Using a New Modeling Workflow

Phillip Tran, Andrian Sue, Paul Wong, Qing Li*, and Paul Carter

***Abstract*—The current conduction pathways resulting from monopolar stimulation of the cochlear implant were studied by developing a human electroanatomical total head reconstruction (namely, HEATHER). HEATHER was created from serially sectioned images of the female Visible Human Project dataset to encompass a total of 12 different tissues, and included computer-aided design geometries of the cochlear implant. Since existing methods were unable to generate the required complexity for HEATHER, a new modeling workflow was proposed. The results of the finite-element analysis agree with the literature, showing that the injected current exits the cochlea via the modiolus (14%), the basal end of the cochlea (22%), and through the cochlear walls (64%). It was also found that, once leaving the cochlea, the current travels to the implant body via the cranial cavity or scalp. The modeling workflow proved to be robust and flexible, allowing for meshes to be generated with substantial user control. Furthermore, the workflow could easily be employed to create realistic anatomical models of the human head for different bioelectric applications, such as deep brain stimulation, electroencephalography, and other biophysical phenomena.**

***Index Terms*—Bioelectric finite-element analysis, cochlear implant, current conduction, human head model.**

I. Introduction

THE cochlear implant (CI) signifies an important medical technology that has been widely used to treat hearing loss. It works by injecting current into the cochlea to electrically stimulate the sensory neurons [1]. Different modes of stimulation exist, with the most common schemes being monopolar (MP) current stimulation in the form of MP1, MP2, and MP1 + 2 modes [2]. For this, the current is passed from the intracochlear electrode to a remote ground electrode: a ball located in the temporalis muscle (MP1), the plate on the implant body at the back of the head (MP2), or both (MP1 + 2) [3], [4]. However, the specific *in vivo* current pathways have not been studied to date. For ideal CI stimulation, all of the current would flow from the stimulating electrode to the return electrode via the modiolus, thereby exciting the targeted spiral ganglion neurons with a minimum amount of electrical power. Conversely, if the current fails to take the ideal modiolar pathway, then the current is described as "leaked" or lost since it does not contribute to neural activation [5]. While the modiolar pathway is commonly reported in the literature [6], some research has suggested other pathways, such as the round window [6], the facial nerve [6]–[8], the cochlear walls [9], and the jugular vein [10].

Traditional experimental techniques are impractical for investigating *in vivo* current pathways since obtaining the measurements would be highly invasive [11]. Computational modeling is an effective alternative that can determine and visualize these pathways in the context of the anatomy [12]. To date, numerous volume conduction models have examined the current spread within the local cochlea region [12]–[17]. These models, however, do not take into consideration the anatomical structures outside the cochlea, which influence the boundary conditions, and hence, current conduction pathways induced by MP stimulation. A model of the whole human head would provide insight into this topic; unfortunately, very few head models have focused on CI stimulation. Mens *et al.* [9] created a simplified human head model consisting of three layered spheres of varying radii to represent the brain, bone, and scalp regions, but ignored some important anatomical structures. Chen *et al.* [18] took a different approach by creating a more realistic anatomical model of the human head from magnetic resonance images (MRI). However, the large voxel size of the model (3 mm × 3 mm × 3 mm) implied that many small anatomical structures that may be important for the current pathways were omitted.

Modeling the human head is not uncommon in other applications. Numerous models have been used to study a wide range of bioelectric therapies, such as electroconvulsive therapy (ECT) [19], [20], electroencephalography (EEG) [21], [22], transcranial magnetic stimulation [23]–[25], and deep brain stimulation (DBS) [26]. These models vary greatly in anatomical complexity. Similar to Mens *et al.* [9], some of these models simplified the detailed anatomy of the head into layers of spheres or ellipses with different sizes to represent different tissues [26]. Others reconstructed the geometry of the head using computer-aided design (CAD) [24]. Generally speaking, using anatomically realistic models can provide a factor of improvement over those based on simplified geometries or CAD [27]. Noninvasive scanning data, such as MRI and computed tomography (CT) images, have been used to construct head models, but the use of low

Manuscript received August 17, 2014; revised October 11, 2014; accepted October 13, 2014. Date of publication October 22, 2014; date of current version January 16, 2015. This work was supported by the Australian Research Council (ARC) through a Linkage Scheme (LP0776938), and Cochlear Ltd. The work of P. Tran, A. Sue, and P. Wong was supported by the Australian Postgraduate Award (APA). *Asterisk indicates corresponding author.*

P. Tran, A. Sue, and P. Wong are with the School of Aerospace, Mechanical and Mechatronic Engineering, Faculty of Engineering and IT, The University of Sydney, Camperdown NSW 2006, Australia (e-mail: phillip.tran@sydney.edu.au; andrian.sue@sydney.edu.au; paul.wong@sydney.edu.au).

*Q. Li is with the School of Aerospace, Mechanical and Mechatronic Engineering, Faculty of Engineering and IT, The University of Sydney, Camperdown NSW 2006, Australia (e-mail: qing.li@sydney.edu.au).

P. Carter is with the School of Aerospace, Mechanical and Mechatronic Engineering, Faculty of Engineering and IT, The University of Sydney, Camperdown NSW 2006, Australia and also with Cochlear Ltd., Macquarie University, North Ryde NSW 2109, Australia (e-mail: pcarter@cochlear.com).

Color versions of one or more of the figures in this paper are available online at http://ieeexplore.ieee.org.

Digital Object Identifier 10.1109/TBME.2014.2364297

resolution data only allows relatively coarse models to be generated [18], [19]. In addition, a number of studies created head models with few tissues [20], [22], [25]. From a biophysical perspective, the number of tissues included in the model would also affect the accuracy of the model, with more tissues being required to produce more realistic results [21]. As noted by Potratz *et al.* [11] and Lau *et al.* [28], it is critical to represent different levels of anatomical details for accurate bioelectric modeling.

With these considerations, the primary purpose of this study was to create a realistic human electroanatomical total head reconstruction (HEATHER) to better predict the current conduction pathways during MP2 CI stimulation. This mode, with the return electrode at the implant site, was chosen because it is used by all major manufacturers of cochlear implants. The increased complexity of the finite-element (FE) model required a more robust and flexible methodology. As such, the development of a new modeling workflow was the secondary objective of this study.

II. Methodology

A. Creation of HEATHER

1) Anatomical Data Source: Serially sectioned images of the Visible Human Project were obtained with permission from the U.S. National Library of Medicine (National Institutes of Health, Bethesda, MD, USA). The female dataset was chosen because the voxel size (0.33 mm $\times$ 0.33 mm $\times$ 0.33 mm) was smaller than that of the male dataset (1 mm $\times$ 1 mm $\times$ 1 mm), allowing for a more realistic representation of small anatomical features, such as the cochlea [29]. The first 765 images (255 mm) of the dataset representing the head and neck were used in this study. An example of a sectioned image passing through the cochleae is shown in Fig. 1(a).

2) Image Processing: The images were cropped from their original resolution (2048 pixels $\times$ 1216 pixels) to fit the head, with a padding of 1–5 pixels beyond the extremities of the head [see Fig. 1(b)]. The final image resolution was 530 pixels $\times$ 645 pixels (176.67 mm $\times$ 215 mm). The cropping operation removed irrelevant background information, such as the blue gel used to embed the specimen, the grayscale table, and identification number. This reduced the size of the dataset, improving computational efficiency in the subsequent steps.

The remaining blue background of the cropped images was removed by adjusting the RGB (red, green, blue) color values of the pixels using MATLAB (MathWorks Inc., Natick, MA, USA). The process, suggested by Zhao *et al.* [30], relied on the fact that the background gel pixels were defined by higher green and blue color intensity values than that of red. If the green or the blue color value was greater than the red color value for a particular pixel, then the pixel was considered to be a "gel" or "background" pixel, and all three color values were adjusted to zero to make this pixel black. Tissue regions that were affected by this process had their original color values reinstated to ensure the information was not lost. The result is shown in Fig. 1(b).

3) Segmentation: Segmentation was performed using ScanIP v4.3 (Simpleware Ltd., Exeter, U.K.) and Photoshop CS6 (Adobe Systems Inc., San Jose, CA, USA), exposing the tools of both programs and enabling a more flexible and efficient segmentation process. Manual and automatic techniques were employed to complete this task in 2-D (individual images) and 3-D (entire model). The transfer of files between ScanIP and Photoshop involved a small number of steps using ImageJ v1.47 (National Institutes of Health, Bethesda, MD, USA), and ImageMagick v6.8.0 (ImageMagick Studios LLC). All 765 images were segmented into 12 different tissues that were deemed to be significant in the head, as shown in Fig. 1(c)–(f). The perilymph included the cochleae and the semicircular canals, while the nerve included only cranial nerves II, VII, and VIII.

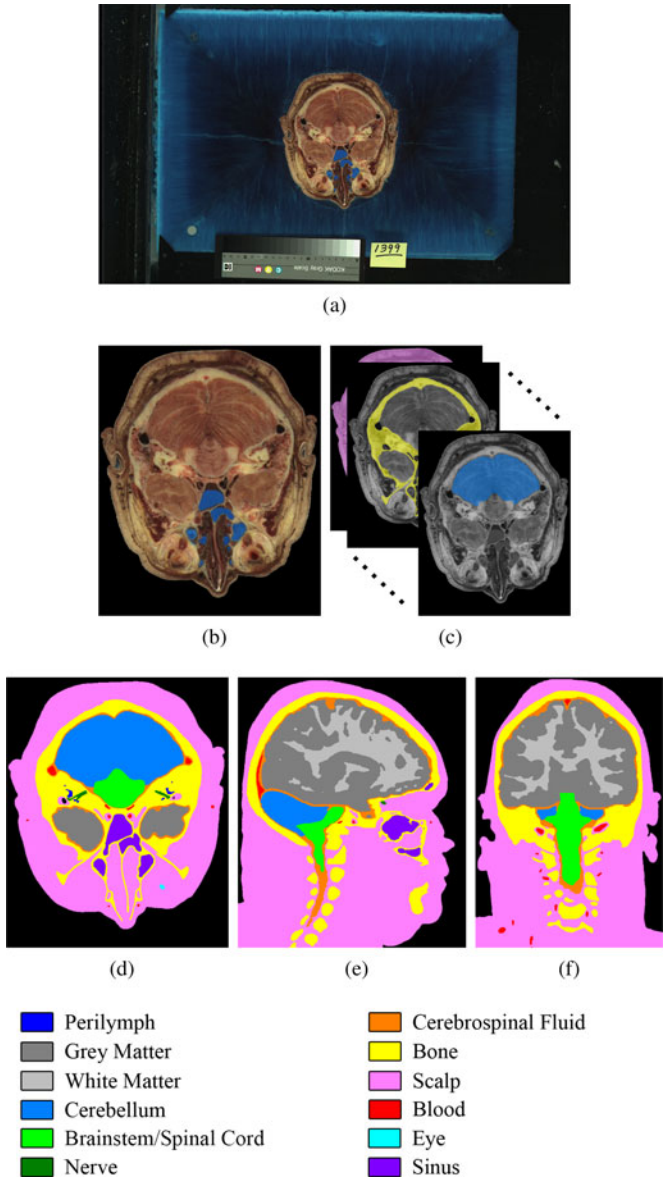

Fig. 1. Image from the Visible Human Project (a) in its original state, and (b) after cropping and processing to remove the background. (c) Segmentation was conducted for 12 tissues (represented by different colors) to obtain the final segmentation as shown in (d) transverse, (e) sagittal, and (f) coronal views.

4) Surface Modeling: Surfaces were created from the segmented dataset in ScanIP. The Stereolithography Rapid Prototyping (STL RP) surface meshing algorithm was used to create a separate surface for each tissue that was conformal with its adjacent structures [see Fig. 2(a)].

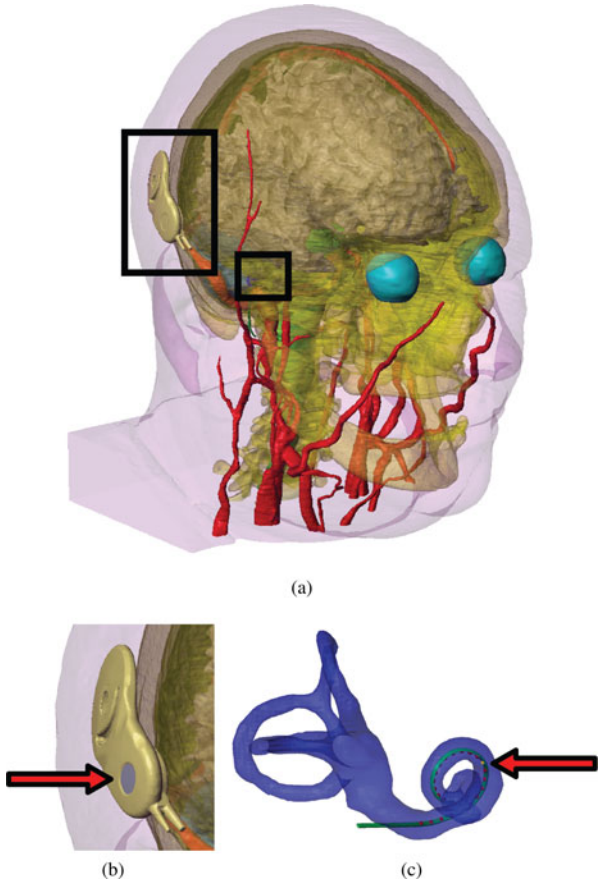

Fig. 2. (a) Transparent 3-D view of HEATHER with 12 tissues, with the implant body and the cochlea highlighted. (b) Close-up view of the implant body with the plate electrode highlighted in blue. (c) Close-up view of the intracochlear electrode array inserted into the cochlea, with the 11th electrode highlighted in yellow.

The CAD geometry of the CI24RE cochlear implant body was obtained from Cochlear Ltd. and added to the model. Care was taken to position the implant body in the scalp tissue behind the ear [see Fig. 2(b)]. This location was chosen to mimic the typical location for the implant body [3]. A simplified geometry of the intracochlear electrode array was created using SolidWorks 2012 (Dassault Systèmes SolidWorks Corp., Waltham, MA, USA), which consisted of a silicone tube that was modeled as a semicircular sweep following the spiral path of the ipsilateral cochlea and 22 hemispherical electrodes embedded in the carrier [see Fig. 2(c)].

5) Volume Meshing: A volumetric tetrahedral mesh was generated in ICEM CFD 14.5 (ANSYS Inc., Canonsburg, PA, USA) using the Octree meshing algorithm (see Fig. 3). Selective mesh refinement was achieved by prescribing the minimum and maximum mesh size for each tissue, as well as varying the Curvature/Proximity Based Refinement (CPBR) value.

ICEM CFD can export the resulting volumetric mesh as different formats required for different FE packages. In this paper, we consider exportation into COMSOL Multiphysics v4.3 (COMSOL AB, Stockholm, Sweden) and ANSYS Multiphysics 14.5 (ANSYS Inc., Canonsburg, PA, USA), respectively, to demonstrate the flexibility of the modeling workflow, and to see if the numerical results were the same. Specifically, the mesh in ICEM CFD was exported as a NASTRAN data file.

TABLE I
ELECTRIC RESISTIVITY FOR DIFFERENT MATERIALS USED IN HEATHER

Material	Resistivity ($\Omega \cdot$m)
Perilymph	0.7
Gray Matter	3
White Matter	7.143
Cerebellum	6.25
Brainstem/Spinal Cord	6.25
Nerve	2.857
Cerebrospinal Fluid	0.56
Bone	76
Scalp	2.38
Blood	1.6
Eye	2
Sinus	16,000
Platinum	1.06×10^{-7}
Silicone	1×10^{7}

B. Simulation of Cochlear Implant Stimulation

1) Simulation in COMSOL Multiphysics: Eight different meshes were created using CPBR values ranging from 1 to 8 and set up in COMSOL for a mesh convergence study. An electrical resistivity was prescribed for each of the tissues (see Table I). Electrical resistivity values were based on those reported in the literature [13], [31]–[40], and assumed to be linear isotropic. Stationary simulations were performed under the assumption that permittivity effects were negligible. As such, the electrical permittivity for all materials was set to a value of 1. The surface representing the plate electrode of the implant body was electrically grounded ($V = 0$) [see Fig. 2(b)]. An electric current terminal of 0.1065 mA was applied to the surface of the 11th intracochlear electrode, situated on the medial side of the cochlea, approximately 180° rotationally from the cochleostomy [see Fig. 2(c)]. This electrode was chosen to replicate a typical stimulus from the cochlear implant. The simulation was computed using the direct PARDISO solver.

2) Simulation in ANSYS Multiphysics: In this platform, only the converged mesh (CPBR $= 5$) was used. The NASTRAN file was imported into the finite-element modeler (FE modeler) module of Workbench 14.5 (ANSYS Inc., Canonsburg, PA, USA) to create a mechanical APDL input file. This file was loaded in ANSYS Multiphysics. The flexible SOLID231 elements were used because they allowed for both linear and quadratic tetrahedral elements. The electrical resistivity (see Table I) and permittivity were defined for each of the different materials for a stationary simulation. The same boundary conditions that were used for COMSOL were applied. The simulation was computed using the direct SPARSE solver.

III. RESULTS

A. HEATHER Volume Mesh

Generation of the volume mesh in ICEM CFD took approximately 1 h on an Intel Core i7 950 desktop computer with 24 GB of RAM. Fig. 3 shows that the new meshing workflow was successful in generating a volume mesh with a good level of

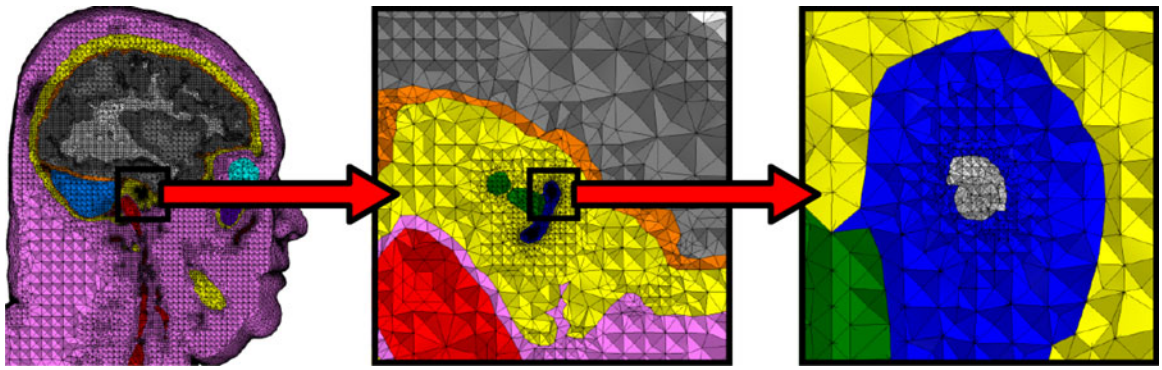

Fig. 3. Sagittal section of the CPBR = 5 mesh showing different levels of zoom of the cochlea region. Regions of high and low mesh density exist.

TABLE II
MESH STATISTICS AND IMPEDANCE VALUES OBTAINED FROM SIMULATION FOR DIFFERENT MESH REFINEMENT LEVELS

Refinement Level (CPBR)	Number of Degrees of Freedom	Number of Elements	Average Aspect Ratio	Impedance (kΩ)
1	564 421	3 309 255	5.142	1.852
2	690 245	4 040 556	5.182	1.873
3	958 887	5 611 950	5.046	1.885
4	1 328 174	7 773 340	4.969	1.886
5	1 605 173	9 348 765	4.962	1.888
6	1 898 342	11 094 983	4.964	1.888
7	2 240 563	13 084 692	4.958	1.885
8	2 548 192	14 873 116	4.934	1.885

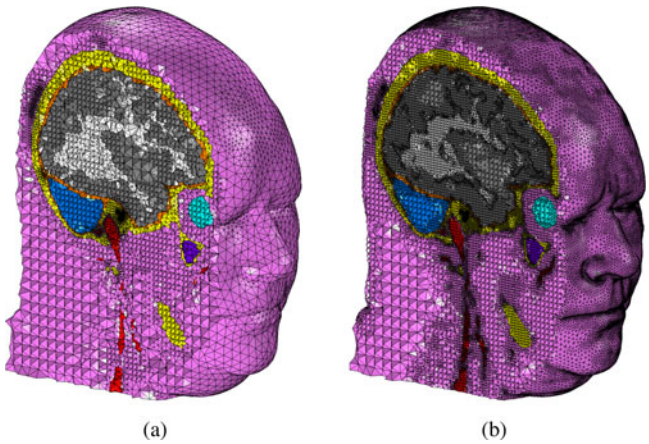

Fig. 4. Isometric view of the sectioned mesh with different levels of refinement. (a) CPBR = 1, and (b) CPBR = 8.

control and smooth transitions between regions of high mesh density and low mesh density. The quality of the mesh was assessed by quantifying the average aspect ratio to assure the accuracy of the solution (see Table II) [41], [42].

B. Convergence Study

Fig. 4(a) and (b) shows two different mesh densities obtained with CPBR values of 1 (least dense) and 8 (most dense), respectively. The number of elements and degrees of freedom obtained through these two different levels of refinement varied significantly, as seen in Table II. It is also noted that in terms of the average aspect ratio, the overall mesh quality improved marginally with increasing mesh refinement.

The time taken to complete the stationary simulation in COMSOL varied from 1 min for CPBR = 1 to 10 min for CPBR = 8. The maximum voltage obtained from these different FE simulations varied by less than 2% and converged to a value of 0.2011 V (1.888 kΩ) for CPBR = 5. Hence, this mesh was used for all subsequent simulations.

C. Comparison Between COMSOL and ANSYS Results

COMSOL and ANSYS voltage and current density contour plots are compared in Fig. 5. The contours are quite similar for both solvers, although the images appear different due to the continuous versus discrete nature of the COMSOL and ANSYS plots, respectively. The maximum voltage for both simulations was 0.2011 V (1.888 kΩ). The simulation time in COMSOL was approximately 5 min, compared to 20 min in ANSYS. For this reason, COMSOL was preferred as the package for all other simulations.

D. Current Conduction Pathways

Current density streamlines were obtained from COMSOL, and are shown in Fig. 6. They indicate the direction of current flow from the stimulating electrode surface to the return electrode. The number of streamlines passing through a particular region is indicative of the amount of current passing through that region. As shown in Fig. 6(a), the current leaves the cochlea predominantly through three different pathways: (A) the modiolus (14% of the current leaving the cochlea through the auditory nerve), (B) the basal end of the cochlea (22% of the current passing through the basal end of the scala tympani and entering the vestibular system), and (C) the cochlea walls (the remaining 64% of the current traveling through the temporal bone). Outside of the cochlea [see Fig. 6(b)], the current conduction can be broadly classified as flowing through either (D) the cranial cavity, or (E) the scalp.

IV. DISCUSSION

A. HEATHER and Current Conduction Pathways

The volume conduction results revealed that a small proportion of current entered the modiolus to induce neural stimulation, before traveling to the ground through the conductive

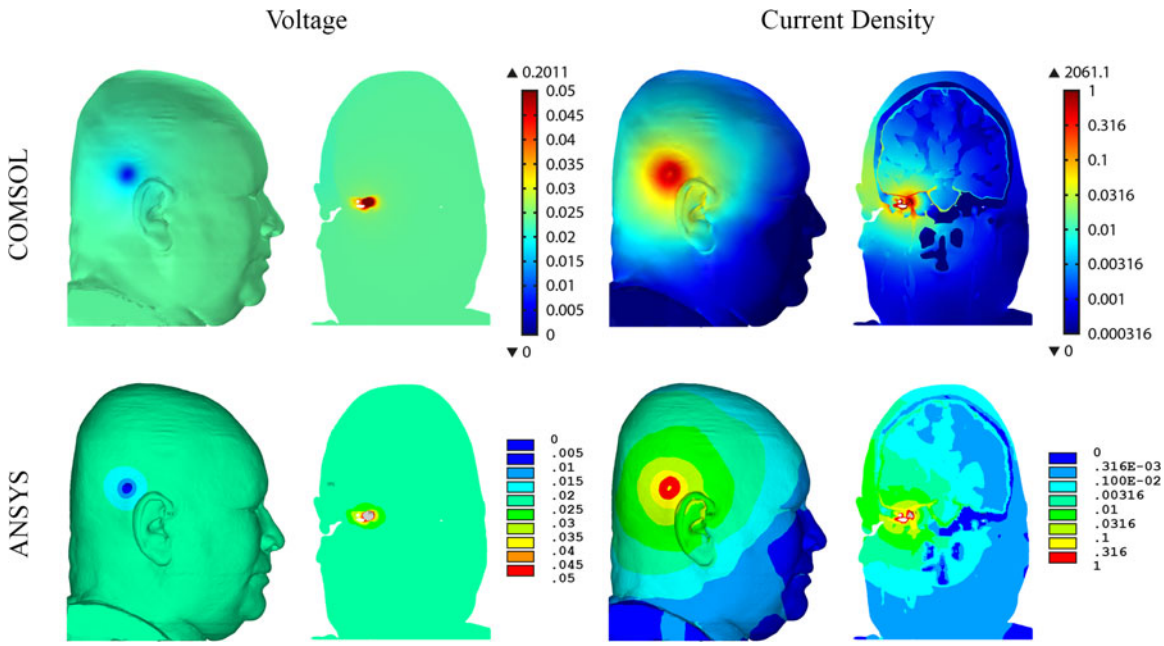

Fig. 5. Contour plots for scalp surface and coronal section view at the cochlea. Plots show voltage and current density from COMSOL (continuous contours) and ANSYS (discrete contours). Note that the contours were scaled to show the greatest dynamic range, and the scales are the same for COMSOL and ANSYS results.

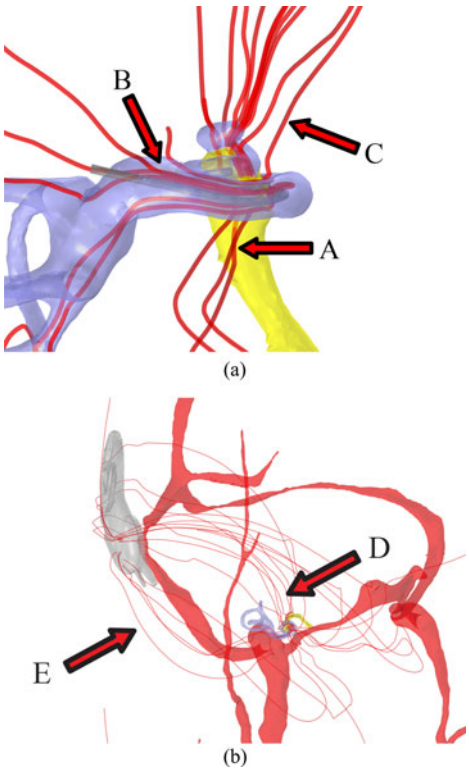

Fig. 6. Current density streamlines originating from the stimulating electrode. (a) Close-up view of the cochlea (blue) and cochlear nerve (yellow). The current is exiting the cochlea via the (A) modiolus, (B) basal end of the cochlea, and (C) cochlea walls. (b) Isometric view of the head with blood vessels (red). The current is passing through the (D) cranial cavity, and (E) scalp.

cerebrospinal fluid of the cranial cavity. The rest of the current exited the cochlea through nonfunctional pathways, and then, passed through the scalp to reach the ground. The pathways found here agreed with those described in the literature [6], [9], however the proportion of current passing through the modiolus is much lower than that measured by Spelman *et al.* (60–75%) [43]. This difference is most likely due to the broad classification of the stimulating and unstimulating paths by Spelman *et al.*, and the assumption that current cannot pass through the resistive bone of the cochlear walls to leave the cochlea.

It has been reported that bioelectric simulation results are sensitive to the tissue geometries [21] and resistivities [34], [37] locally. One of our previous studies [44] showed that small tissues, such as blood vessels, only had small localized effects on the current conduction. It is speculated that large head tissues that are in contact with the cochlea, such as bone, would have a greater effect on the current conduction inside and outside the cochlea. A tissue sensitivity analysis, to be conducted later using HEATHER, will clarify this, thereby gaining quantitative insights into the patient specific variations. In either case, it is important for these geometries and resistivities to be modeled accurately.

The main problem with existing cochlea sized models is that it is difficult to assign boundary conditions that would accurately replicate the results of a model that included larger tissues. One possible solution to this would be to capture the geometric and anatomic details of CI stimulation with a high-resolution cochlea region and a lower resolution head region (a multiscale study). Following this, the current distributions within the cochlea and their exit paths could be analyzed more effectively.

Regardless of the geometric and anatomic complexity of the model, it is important to validate HEATHER to ensure the simulation results are accurate and reliable. In addition, HEATHER was created from the female dataset of the Visible Human Project, making it a patient-specific model. The results obtained from HEATHER should be generalizable for the population of

CI recipients in order for it to be a useful tool in the prediction of current conduction. The validation technique proposed, to be published later, involves the recording of scalp potentials, or impedances, of recipients at various points on the head during CI stimulation. The impedance across the electrode-tissue interface is expected to be 4–10 kΩ [45], [46], more than double the value of 1.888 kΩ obtained using HEATHER. This is mainly due to the polarization voltage being ignored in the stationary simulation [47].

The Visible Human Project dataset contained some undesired image artifacts that made segmentation somewhat difficult. Some small anatomical structures were missing as a result of the acquisition process, including part of the temporal lobe of the brain, and the chin [48]. In addition, some parts of the scalp were deformed, these being two large vertical wrinkles on the anterior surface of the scalp, an indent on the top of the head, and the back of the head being flat. Manual intervention was sometimes required to create HEATHER with a more realistic geometry.

The segmentation of HEATHER did not include the otic capsule, a layer of dense bone surrounding the cochlea with an average thickness of approximately 1 mm [8]. The resistivity of the otic capsule is higher than that of typical bone [8], so the current exiting the cochlea through the cochlea walls is possibly overestimated. Hence, the real amount of current taking the modiolar pathway could be greater than that currently predicted by HEATHER. Furthermore, otosclerosis is a condition where the density, and therefore, resistivity, of the otic capsule is reduced [8], [49]. The amount of current exiting the cochlea via the cochlea walls is expected to increase for patients suffering from this condition [9]. This has implications for facial nerve stimulation, as the facial nerve passes close to the cochlea spiral, in particular the geniculate ganglion [50]. As described by Vanpoucke *et al.* [7] and Frijns *et al.* [8], facial nerve stimulation is a common side effect of current injection by the cochlear implant, making it important to accurately model these effects to better understand, and consequently, reduce their occurrence.

HEATHER's simplified cochlear implant components may have affected the current conduction results. Control of the implant body position in the scalp tissue was restricted because limited tools were available for moving parts in ICEM CFD. As such, a trial-and-error procedure was required to ensure that the implant body was not exposed. It was also assumed that the simplified intracochlear electrode array geometry would not impact on the far-field current conduction pathways. To investigate the effects of the electrode array geometry on current conduction within the cochlea, a high-resolution model of the cochlea would be required.

B. Modeling Workflow

The various processes of the modeling workflow led to the use of multiple software packages in this study. The packages described in this paper were chosen based on their availability and popularity. In other words, it would be possible to follow a similar procedure accommodating other programs and tools. In addition, the use of multiple software packages meant that many steps were involved in the data transfer between different programs. While each of these steps was relatively simple, the entire process could be slower than ideal.

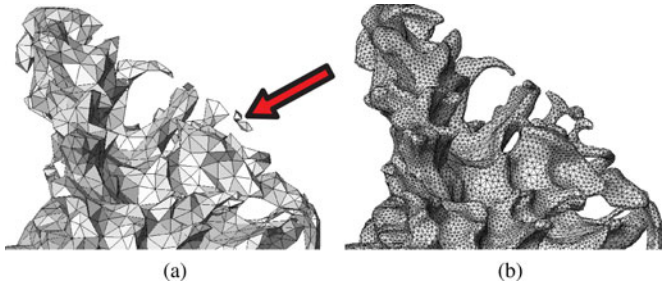

Fig. 7. Close-up view of the white matter mesh with different levels of refinement. (a) CPBR = 1, and (b) CPBR = 8. Fragmentation of the mesh is evident in the pointed region.

Many meshing programs allow the user to vary the mesh density in different regions of the model. From this study, it was found that ICEM CFD was more robust and provided greater control over mesh density for different parts of the head model. This proved to be especially useful for HEATHER, as both coarse and fine anatomical details were desired. Small structures, such as the platinum electrodes of the intracochlear electrode array, required a fine mesh to properly capture the geometry. On the other hand, a coarse mesh was sufficient to represent the geometry of larger structures. Meshing in this way provided a combination of accuracy in the regions that were deemed critically important, and efficiency in overall computational cost.

Controlling the mesh density was achieved by varying the CPBR value in ICEM CFD. The CPBR value defined the number of elements representing curved regions, and therefore, the total number of elements and degrees of freedom in HEATHER. Small, detailed anatomical structures, such as blood vessels and white matter, were affected more than large structures. As shown in Fig. 7(a) and (b), some regions of the white matter are fragmented with low mesh density (CPBR = 1), but are connected with a high mesh density (CPBR = 8). These considerable changes in mesh density did not result in significant changes in the impedance (<2%), suggesting the discretization was well converged. In addition, the average element aspect ratio obtained for the different meshes did not change significantly (<5%). However, it has been suggested that meshes with an average aspect ratio greater than 5 may have issues with accuracy [51], providing a reason for selecting the CPBR = 5 mesh.

In some instances, the fragmentation could not be resolved by generating a denser mesh in ICEM CFD. Various components of the mesh became disjointed, often forming very small parts with as few as one element. Assigning properties to these parts was problematic as each part required manual inspection, and the user's knowledge and familiarity with the dataset and segmentation. In addition, jagged edges were formed in regions where more than two components came together when meshing in ICEM CFD. While this was acceptable for the model used in this study, it may create undesirable concentrations for other applications.

The FE mesh was exported into two different FE packages to test the flexibility and feasibility of the modeling workflow. ICEM CFD was capable of exporting various file types,

allowing different FE packages to be used, such as ABAQUS. The results from the two tested models in COMSOL and ANSYS were identical to three significant figures, which cross-checked the correctness and accuracy. The voltage and current density distributions, as well as the maximum voltage measurements, were the same.

Although the modeling workflow was used to create HEATHER for electric conduction induced by a CI, other applications could also take advantage of it. For example, the modeling workflow can easily be adapted to other areas, such as DBS and EEG, where electric conduction in a head model is critical. It is projected that the flexibility of the modeling workflow not only applies for different simulation packages, but also for simulations targeting other physical quantities. This includes, but is not limited to, structural (head impact), magnetic (MRI examination), thermal, and coupled physics (cell phone radiation). The user can create an anatomical model, with relevant implant geometries if required, and be able to mesh and solve the specific problem efficiently.

V. Conclusion

A new modeling workflow was proposed in this study. The procedure proved to be robust and flexible for the creation of patient-specific finite element (FE) models. The new workflow was used to create HEATHER for modeling monopolar (MP) stimulation of the cochlear implant (CI). Three major pathways were identified for current to leave the cochlea during CI stimulation, which match well with those described in the literature. Two current conduction pathways through the head were also identified. It is possible to study different aspects of CI stimulation with HEATHER for better design and implementation of CI arrays. The established workflow also makes it possible to create better models for many other applications with different physics. Additionally, different programs can be accommodated in each stage of the proposed modeling workflow.

Acknowledgment

The authors would like to thank the U.S. National Library of Medicine (National Institutes of Health) for providing access to the Visible Human Project datasets that were used to produce the model described here.

References

[1] B. S. Wilson and M. F. Dorman, "Cochlear implants: A remarkable past and a brilliant future," *Hearing Res.*, vol. 242, no. 1–2, pp. 3–21, 2008.

[2] B. S. Wilson and M. F. Dorman, "The design of cochlear implants," in *Cochlear Implants: Principles & Practices*, J. K. Niparko, Ed. Philadelphia, PA, USA: Lippincott Williams & Wilkins, 2009.

[3] G. M. Clark, *Cochlear Implants: Fundamentals and Application*. R. T. Beyer, Ed. New York, NY, USA: Springer-Verlag, 2003.

[4] F. G. Zeng, S. Rebscher, W. Harrison, X. Sun, and H. Feng, "Cochlear implants: System design, integration, and evaluation," *IEEE Rev. Biomed. Eng.*, vol. 1, pp. 115–142, Nov. 2008, DOI: 10.1109/RBME.2008.2008250

[5] J. H. Schulman, D. I. Whitmoyer, J. C. Gord, and P. Strojnik, "Multichannel cochlear implant system including wearable speech processor" U. S. Patent *5 603 726*, Feb. 18, 1997.

[6] A. G. Micco and C. P. Richter, "Tissue resistivities determine the current flow in the cochlea," *Curr. Opin. Otolaryngo.*, vol. 14, no. 5, pp. 352–355, 2006.

[7] F. Vanpoucke, A. Zarowski, J. Casselman, J. Frijns, and S. Peeters, "The facial nerve canal: An important cochlear conduction path revealed by Clarion electrical field imaging," *Otol. Neurotol.*, vol. 25, no. 3, pp. 282–289, 2004.

[8] J. H. M. Frijns, R. K. Kalkman, and J. J. Briaire, "Stimulation of the facial nerve by intracochlear electrodes in otosclerosis: a computer modeling study," *Otol. Neurotol.*, vol. 30, no. 8, pp. 1168–1174, 2009.

[9] L. H. M. Mens, G. Huiskamp, T. Oostendorp, and P. van den Broek, "Modelling surface potentials from intracochlear electrical stimulation," *Scand. Audiol.*, vol. 28, no. 4, pp. 249–255, 1999.

[10] P. Tran, Q. Li, and P. Carter, "Finite element modeling of current flow from cochlear implant stimulation," in *Proc. IASTED Int. Conf. Modelling, Simulation, Identification*, Pittsburgh, PA, USA, 2011, pp. 436–442.

[11] C. Potratz, S. Petersen, A. Grünbaum, and U. van Rienen, "Challenges in bio-electromagnetic modeling," presented at the 2010 URSI Int. Symp. Electromagn. Theory, Berlin, Germany, Aug. 16–20, 2010, pp. 344–347.

[12] G. Girzon, "Investigation of current flow in the inner ear during electrical stimulation of intracochlear electrodes," M.S. thesis, Dept. Elect. Eng. and Comp. Sci., Massachusetts Institute of Technology, Cambridge, MA, USA, 1987.

[13] C. C. Finley, B. S. Wilson, and M. W. White, "Models of neural responsiveness to electrical stimulation," in *Cochlear Implants: Models of the Electrically Stimulated Ear*, J. M. Miller, and F. A. Spelman, Ed. New York, NY, USA: Springer-Verlag, 1990, pp. 55–96.

[14] J. H. M. Frijns, J. J. Briaire, and J. J. Grote, "The importance of human cochlear anatomy for the results of modiolus-hugging multichannel cochlear implants," *Otol. Neurotol.*, vol. 22, no. 3, pp. 340–349, 2001.

[15] T. Hanekom, "Three-dimensional spiraling finite element model of the electrically stimulated cochlea," *Ear Hearing*, vol. 22, no. 4, pp. 300–315, 2001.

[16] C. T. M. Choi, W. D. Lai, and Y. B. Chen, "Optimization of cochlear implant electrode array using genetic algorithms and computational neuroscience models," *IEEE Trans. Magn.*, vol. 40, no. 2, pp. 639–642, Mar. 2004.

[17] P. Wong, Q. Li, and P. Carter, "Incorporating vascular structure into electric volume conduction models of the cochlea," in *Proc. IEEE EMBS Conf. Biomed. Eng. Sci.*, Langkawi, Malaysia, 2012, pp. 694–699.

[18] K. Chen, Q. Li, W. Li, H. Lau, A. Ruys, and P. Carter, "Three-dimensional finite element modeling of cochlear implant induced electrical current flows," presented at the IEEE Int. Conf. Computational Intelligence for Measurement Systems and Applications, Hong Kong, China, May 11–13, 2009.

[19] S. Bai, C. Loo, A. Al Abed, and S. Dokos, "A computational model of direct brain excitation induced by electroconvulsive therapy: comparison among three conventional electrode placements," *Brain Stimul.*, vol. 5, no. 3, pp. 408–421, 2012.

[20] W. H. Lee, Z. D. Zeng, T. S. Kim, A. F. Laine, S. H. Lisanby, and A. V. Peterchev, "Regional electric field induced by electroconvulsive therapy in a realistic finite element head model: Influence of white matter anisotropic conductivity," *NeuroImage*, vol. 59, no. 3, pp. 2110–2123, 2012.

[21] C. Ramon, P. H. Schimpf, and J. Haueisen, "Influence of head models on EEG simulations and inverse source localizations," *Biomed. Eng. Online*, vol. 5, no. 10, 2006.

[22] D. Güllmar, J. Haueisen, and J. R. Reichenbach, "Influence of anisotropic electrical conductivity in white matter tissue on the EEG/MEG forward and inverse solution. A high-resolution whole head simulation study," *NeuroImage*, vol. 51, no. 1, pp. 145–163, 2010.

[23] M. Nadeem, T. Thorlin, O. P. Gandhi, and M. Persson, "Computation of electric and magnetic simulation in human head using the 3-D impedance method," *IEEE Trans. Biomed. Eng.*, vol. 50, no. 7, pp. 900–907, Jul. 2003.

[24] T. A. Wagner, M. Zahn, A. J. Grodzinsky, and A. Pascual-Leone, "Three-dimensional head model simulation of transcranial magnetic stimulation," *IEEE Trans. Biomed. Eng.*, vol. 51, no. 9, pp. 1586–1594, Sep. 2004.

[25] M. Chen and D. J. Mogul, "Using increased structural detail of the cortex to improve the accuracy of modeling the effects of transcranial magnetic stimulation on neocortical activation," *IEEE Trans. Biomed. Eng.*, vol. 57, no. 5, pp. 1216–1226, May 2010.

[26] P. F. Grant and M. M. Lowery, "Electric field distribution in a finite-volume head model of deep brain stimulation," *Med. Eng. Phys.*, vol. 31, no. 9, pp. 1095–1103, 2009.

[27] F. Vatta, F. Meneghini, F. Esposito, S. Mininel, and F. Di Salle, "Realistic and spherical head modeling for EEG forward problem solution: A comparative cortex-based analysis," *Comput. Intell. Neurosci.*, vol. 2010, pp. 972060-1–972060-11, 2010.

[28] H. Lau, A. J. Ruys, P. Carter, X. Wang, and Q. Li, "Subject specific modelling of electrical conduction in the body: A case study," *J. Biomim. Biomat. Tissue Eng.*, vol. 10, pp. 43–53, 2011.
[29] E. Erixon, H. Högstorp, K. Wadin, and H. Rask-Andersen, "Variational anatomy of the human cochlea: Implications for cochlear implantation," *Otol. Neurotol.*, vol. 30, pp. 14–22, 2009.
[30] Y. Zhao, C. J. Tao, X. L. Tian, and X. S. Tang, "A new segmentation algorithm for the visible human data," in *Proc. IEEE Eng. Med. Biol. Soc.*, Shanghai, China, 2005, pp. 1646–1649.
[31] P. M. Bonovas, G. A. Kyriacou, and J. N. Sahalos, "A realistic three dimensional FEM of the human head," *Physiol. Meas.*, vol. 22, no. 1, pp. 65–76, 2001.
[32] R. N. Holdefer, R. Sadleir, and M. J. Russell, "Predicted current densities in the brain during transcranial electrical stimulation," *Clin. Neurophysiol.*, vol. 117, no. 6, pp. 1388–1397, 2006.
[33] L. A. Geddes and L. E. Baker, "The specific resistance of biological material—A compendium of data for the biomedical engineer and physiologist," *Med. Biol. Eng.*, vol. 5, no. 3, pp. 271–293, 1967.
[34] J. Haueisen, C. Ramon, M. Eiselt, H. Brauer, and H. Nowak, "Influence of tissue resistivities on neuromagnetic fields and electric potentials studied with a finite element model of the head," *IEEE Trans. Biomed. Eng.*, vol. 44, no. 8, pp. 727–735, Aug. 1997.
[35] P. Schimpf, J. Haueisen, C. Ramon, and H. Nowak, "Realistic computer modelling of electric and magnetic fields of human head and torso," *Parallel Comput.*, vol. 24, no. 9–10, pp. 1433–1460, 1998.
[36] S. K. Law, "Thickness and resistivity variations over the upper surface of the human skull," *Brain Topogr.*, vol. 6, no. 2, pp. 99–109, 1993.
[37] M. R. Bashar, Y. Li, and P. Wen, "Effects of local tissue conductivity on spherical and realistic head models," *Australas. Phys. Eng. S.*, vol. 33, no. 3, pp. 233–242, 2010.
[38] K. A. Awada, D. R. Jackson, S. B. Baumann, J. T. Williams, D. R. Wilton, P. W. Fink, and B. R. Prasky, "Effect of conductivity uncertainties and modeling errors on EEG source localization using a 2-D model," *IEEE Trans. Biomed. Eng.*, vol. 45, no. 9, pp. 1135–1145, Sep. 1998.
[39] S. B. Baumann, D. R. Wozny, S. K. Kelly, and F. M. Meno, "The electrical conductivity of human cerebrospinal fluid at body temperature," *IEEE Trans. Biomed. Eng.*, vol. 44, no. 3, pp. 220–223, Mar. 1997.
[40] D. Halliday, R. Resnick, and K. S. Krane, *Physics*, vol. 2, 5th ed. New York, NY, USA: Wiley, 2002.
[41] D. L. Logan, *A First Course in the Finite Element Method*, 4th ed. Toronto, Canada: Thomson, 2007.
[42] P. M. Knupp, "Achieving finite element mesh quality via optimization of the Jacobian matrix norm and associated quantities. Part I—A framework for surface mesh optimization," *Int. J. Numer. Meth. Eng.*, vol. 48, no. 3, pp. 401–420, 2000.
[43] F. A. Spelman, B. M. Clopton, and B. E. Pfingst, "Tissue impedance and current flow in the implanted ear. Implications for the cochlear prosthesis," *Ann. Otol. Rhinol. Laryngol.*, vol. 91, no. 5, pp. 3–8, 1982.
[44] P. Tran, P. Wong, A. Sue, Q. Li, and P. Carter, "Influence of blood vessel conductivity in cochlear implant stimulation using a finite element head model," presented at the IEEE 35th Annu. Int. Conf. Eng. Med. Biol. Soc., Osaka, Japan, Jul. 03–07, 2013.
[45] M. L. Hughes, K. R. V. Werff, C. J. Brown, P. J. Abbas, D. M. R. Kelsay, H. F. B. Teagle, and M. W. Lowder, "A longitudinal study of electrode impedance, the electrically evoked compound action potential, and behavioral measures in Nucleus 24 cochlear implant users," *Ear Hearing*, vol. 22, no. 6, pp. 471–486, 2001.
[46] G. Paasche, F. Bockel, T. Tasche, A. Lesinski-Schiedat, and T. Lenarz, "Changes of postoperative impedances in cochlear implant patients: the short-term effects of modified electrode surfaces and intracochlear corticosteroids," *Otol. Neurotol.*, vol. 27, no. 5, pp. 639–647, 2006.
[47] C. R. Butson and C. C. McIntyre, "Tissue and electrode capacitance reduce neural activation volumes during deep brain stimulation," *Clin. Neurophysiol.*, vol. 116, no. 10, pp. 2490–2500, 2005.
[48] V. Spitzer, M. J. Ackerman, A. L. Scherzinger, and D. Whitlock, "The visible human male: a technical report," *J. Amer. Med. Inform. Assn.*, vol. 3, no. 2, pp. 118–130, 1996.
[49] A. Bozorg Grayeli, C. Saint Yrieix, Y. Imauchi, F. Cyna-Gorse, E. Ferrary, and O. Sterkers, "Temporal bone density measurements using CT in otosclerosis," *Acta Otolaryngol.*, vol. 124, no. 10, pp. 1136–1140, 2004.
[50] R. Ramsden, L. Rotteveel, D. Proops, S. Saeed, A. van Olphen, and E. Mylanus, "Cochlear implantation in otosclerotic deafness," *Adv. Otorhinolaryngol.*, vol. 65, pp. 328–334, 2007.
[51] J. T. Mottram, and C. T. Shaw, *Using Finite Elements in Mechanical Design*. Berkshire, U.K.: McGraw-Hill, 1996.

Phillip Tran received the B.E. (Mech. Eng. (Biomed.)) (Hons I) degree and the B.Sc. (Adv) degree in chemistry from The University of Sydney, Camperdown, Australia, in 2010. He is currently working toward the Ph.D. degree in biomedical engineering at the same university in conjunction with Cochlear Ltd.

His research interests include computational modeling of the human head for cochlear implant stimulation.

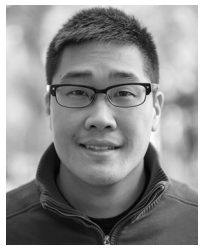

Andrian Sue received the B.E. (Mech. Eng. (Biomed.)) (Hons I) degree and the B.Med.Sc. degree from The University of Sydney, Camperdown, Australia, in 2010. He is currently working toward the Ph.D. degree in biomedical engineering at the same university in conjunction with Cochlear Ltd.

His research interests include computational modeling of electrode–tissue interfaces.

Paul Wong received the B.E. (Mech. Eng. (Biomed.)) (Hons I) degree and the B.Com. degree in finance from The University of Sydney, Camperdown, Australia, in 2010. He is currently working toward the Ph.D. degree in biomedical engineering at the same university in conjunction with Cochlear Ltd.

His research interests include computational modeling of the cochlea for cochlear implant stimulation.

Qing Li received the Ph.D. degree in aerospace engineering from The University of Sydney, Camperdown, Australia, in 2000.

Following Ph.D., he was a Postdoctoral Research Fellow at Cornell University, Ithaca, NY, USA, before returning to The University of Sydney, in 2001 as an Australian Postdoctoral Fellow. He was a Senior Lecturer at James Cook University, Townsville, Australia, in 2004, and then, at The University of Sydney in 2006. He became an Associate Professor in the School of Aerospace, Mechanical and Mechatronic Engineering, The University of Sydney, in 2010. He is currently an ARC Future Fellow and Professor in biomedical engineering at The University of Sydney.

His current research interests include computational modeling, biomechanics, biomaterials, scaffold tissue engineering, crashworthiness, and design optimization.

Paul Carter received the B.S. degree in physics with solid state electronics from the University of Exeter, U.K., in 1982, and the Ph.D. degree in microelectronics at the University of Southampton, Southampton, U.K., in 1987.

He was a Test Engineer at Texas Instruments and worked under a one-year research contract with Plessey Electronics Research PLC, Romsey, U.K., in the area of testing high-density MOS RAMs.

In 1987, he became a Teacher in the Department of Electrical and Computer Engineering at the University of Wollongong, Wollongong, Australia. After five years at the University, he joined Cochlear Ltd., Sydney, Australia, where he works in the area of cochlear implant electrodes and the safety of electrical stimulation.